Supporting Information

Direct carbonization of organic solvent toward graphene quantum dots

Hongji Liu,[a,b,c] ‡ *Xiaotong Lv,*[a,b,d] ‡ *Changwei Li,*[e] ‡ *Yong Qian,*[a,c] *Xingyu Wang,*[a,b,c] *Lin Hu,*[a,c] *Yucai Wang,*[b] *Wenchu Lin,*[a,d]* *Hui Wang,*[a,c,d]*

[a.] High Magnetic Field Laboratory, Chinese Academy of Sciences, Hefei 230031, Anhui, P. R. China. E-mail: wenchu@hmfl.ac.cn; hw39@hmfl.ac.cn.

[b.] University of Science and Technology of China, Hefei, 230026, Anhui, P. R. China.

[c.] The Anhui Key Laboratory of Condensed Matter Physics at Extreme Conditions, Hefei Institutes of Physical Science, Chinese Academy of Sciences, Hefei 230031, Anhui, P. R. China.

[d.] Key Laboratory of High Magnetic Field and Ion Beam Physical Biology, Hefei Institutes of Physical Science, Chinese Academy of Sciences, Hefei 230031, Anhui, China.

[e.] Shanghai Key Laboratory for Prevention and Treatment of Bone and Joint Diseases with Integrated Chinese-Western Medicine, Shanghai Institute of Traumatology and Orthopedics, Ruijin Hospital, School of Medicine, Shanghai Jiaotong University, Huangpu Qu, SH 200025, P. R. China.

‡These authors contributed equally to this work.

Experimental Section

Materials: All chemical reagents were used as received without further purification. Ethylenediamine (En, Ar, ≥99.0%), glycerol (Gl Ar, ≥99.0%), ethylene glycol (Eg, Ar, 99%), dimethyl formamide (Dmf, Ar, 99.0%), acetone (Ac, Ar, ≥99.5%), toluene (To, Ar, ≥99.5%), methanol (Me, Ar, ≥99.7%), ethanol (Et, Ar, ≥99.7%) and carbon tetrachloride (Ct, Ar, 99.5%) were purchased from Aladdin Chemical Co. Ltd. (Shanghai, China). The water used in all experiments was of Millipore Milli-Q grade.

Synthesis of Graphene Quantum Dots from Different Organic Solvents: Typically, 30 mL organic solvents (En, Gl, Eg, Dmf, Ac, To, Me, Et, and Ct) were transferred to a poly(tetrafluoroethylene) (Teflon)-lined autoclave (50 mL) and heated in oven (Shanghai Ke Heng Industrial Co., Ltd.) at 220 ºC. After 24 h, the autoclave was naturally cooled to room temperature. The names of resultant products were defined as GQDs-X, where X represents the abbreviation of different organic solvents. In addition, the decomposition of these organic solvents at different temperature (140, 160, 180, 200, and 240 ^{o}C) had been studied.

To remove the unreacted organic solvents, the as-synthesized GQDs from different precursors were purified through different pots-treatment processes based on the otherness in physical and chemical properties of organic solvents. The unreacted En and Dmf in the resultant products were removed by vacuum distillation, and the GQDs-En and GQDs-Dmf solution was collected by rinsing the round bottom flask with deionized water. The unreacted Gl, To, and Eg in the resultant products were removed by vacuum column chromatography and the GQDs-Gl, GQDs-To, and GQDs-Eg solutions were collected by using deionized water as eluent. The unreacted Ac in the resultant products was dialyzed for 3 days using cellulose ester dialysis bag (molecular weight cutoff (MWCO) = 1000) at room temperature. The GQDs-Ac solution was collected and then concentrated to 10 ml through a heating

treatment. All GQDs solid could be obtained from the solution via freeze-drying. The aqueous dispersion and solid samples of the resultant GQDs were respectively collected for next use.

Characterization: Atomic force microscopy (AFM) analyses were performed on a stand-alone AFM system (Model MFP-3D, Asylum Research, Santa Barbara, CA). High-resolution transmission electron microscopy (HRTEM) images were obtained using a JEOL JEM 2100 system with an acceleration voltage of 200 kV. Raman scattering measurements were performed using a Horiba Jobin YvonT64000 Micro-Raman instrument with a torus 532 laser (λ = 532 nm) as an excitation source in backscattering geometry. A back-illuminated charge-coupled device (CCD) cooled by liquid nitrogen was used to detect the scattered light. The Fourier transform infrared (FT-IR) spectrum was recorded with a Nicolet Instrument Co. iS10 FT-IR spectrometer. The PL study was carried out on a Horiba Jobin Yvon Co. Fluorolog-3-21 spectrofluorometer. The UV-vis spectrum was obtained on an ultraviolet-visible (UV-vis) spectrophotometer (UV 2550, Shimadzu Co., Japan). X-ray electron spectroscopy was performed on an ESCALAB 250 X-ray photoelectron spectrometer with Al Kα radiation. Vacancy structure were detected using the EPR technique (Bruker EMX plus 10/12, eruipped with Oxford ESR 910 Liquid Helium cryostat.).

In Vitro Cell Viability of GQDs-Eg, GQDs-Ac and GQDs-To: Both human cell lines including cervical cancer cells (Hela) and small cell lung cancer cells (NCI-H196) were seeded in a 96-well plate and incubated overnight in RPMI-1640 media supplemented with 10% fetal bovine serum and 1% penicillin/streptomycin. On the following day, the medium was replaced with a medium containing GQDs-Eg, GQDs-Ac or GQDs-To, or with PBS (control), respectively. Each sample at different concentrations (25, 50, 100 and 200 $\mu g\ mL^{-1}$) was run in sextuplicate. Cells were incubated with GQDs for 72 h. Cells in wells containing the medium without GQDs were used as the control. Cell viability was assessed by using a CellTiter-Glo Luminescent assay (Promega, Madison, WI, USA). Luminescence was measured in a multilabel plate reader (Envision PerkinElmer, USA). The fluorescence

intensity from GQDs-Eg, GQDs-Ac, or GQDs-To treated cells was compared to the intensity from PBS-treated control cells to determine percent viability.

In vitro Confocal Imaging: Hela cells were seeded onto glass coverslips in a 6-well plate. After overnight incubation, cells were incubated with GQDs-Eg, GQDs-Ac or GQDs-To (50 μg/mL) for 4h, respectively. Cells were then washed with cold PBS three times and fixed with 4% paraformaldehyde for 15 min at 37 ^{o}C. Cells were then mounted onto glass slides with ProLong® Gold Antifade Mountant (Life Technologies Inc., Gaithersburg, MD). The imaging of cells was acquired using an FV1200MPE laser scanning microscope (Olympus Corporation, Japan) at different excitation wavelengths, including 405, 488, and 546 nm.

In Vitro Two-photon Fluorescent Imaging: Hela cells were seeded onto glass coverslips in a 24-well plate. After 24 h, cells were incubated with GQDs-Eg, GQDs-Ac or GQDs-To (50 μg/mL) for 4 h, respectively. Cells were then washed with PBS three times and fixed with 4% paraformaldehyde for 10 min. Nuclei were stained with 4′,6-diamidino-2-phenylindole (DAPI) before cells were mounted onto glass slides with ProLong® Gold Antifade Mountant (Life Technologies Inc., Gaithersburg, MD). Two-photon imaging was performed using a multiphoton microscope (Leica TCS SP8, Germany) with an excitation wavelength of 800 nm.

Histopathological Evaluation of organs from mice treated with GQDs-Eg, GQDs-Ac or GQDs-To: After being intravenously injected for five days using PBS injection (control) or GQDs-Eg, GQDs-Ac or GQDs-To (1 mg mL^{-1}, dispersed in PBS), male ICR mice with six weeks old (Beijing Vital River Laboratory Animal Technology Co., Ltd, China) were euthanized and whole organs (heart, liver, spleen, lung, and kidney) were removed and preserved in 4% paraformaldehyde for 24 h. PBS-treated mice were used as control. Tissues were then embedded in paraffin, sliced into 5 μm sections, and stained with hematoxylin and eosin (H&E).

Hematology Assay: After being intravenously injected for 24 h using GQDs-Eg, GQDs-Ac or GQDs-To (1 mg mL^{-1}, dispersed in PBS), 3mL of blood was drawn from mice (n = 4) via the

cardiac puncture method after deep terminal anesthesia. PBS-treated mice (n = 4) were used as control. Collected samples were sent to Nanjing Biomedical Research Institute of Nanjing University for analysis.

Supplementary text

The relative PL QY of contrast agent is the usually the ratio of the emitted photons to the absorbed photons.[1] It can be led to

$$QY = QY_{ref}\frac{\eta^2 \quad I \quad A_{ref}}{\eta_{ref}^2 I_{ref} \quad A}$$

where QYref is the QY of rhodamine B dissolved in ethanol as a reference, η is the refractive index of H_2O = 1.3333 (η_{ref} of ethanol = 1.361), I is the integrated PL intensity and A is the absorbance at the excitation wavelength. The absolute PL QY was measured and estimated.

Supplementary figures

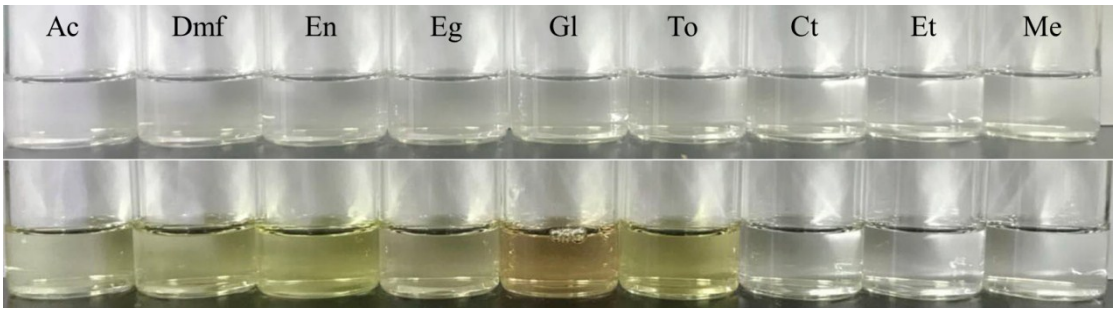

Fig. S1. Optical photograph of organic solvents before (top) and after (down) being treated by a thermal process at 220 ^{o}C for 24 h.

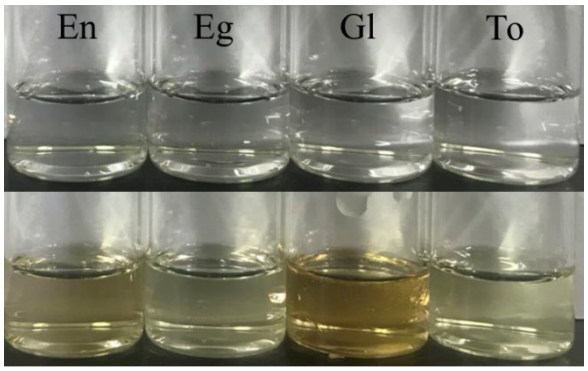

Fig. S2. Optical photograph of organic solvents before (top) and after (down) being treated by a thermal process at 140 ^{o}C for 24 h.

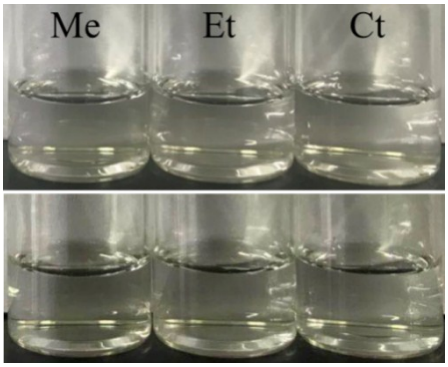

Fig. S3. Optical photograph of organic solvents before (top) and after (down) being treated by a thermal process at 240 ^{o}C for 24 h.

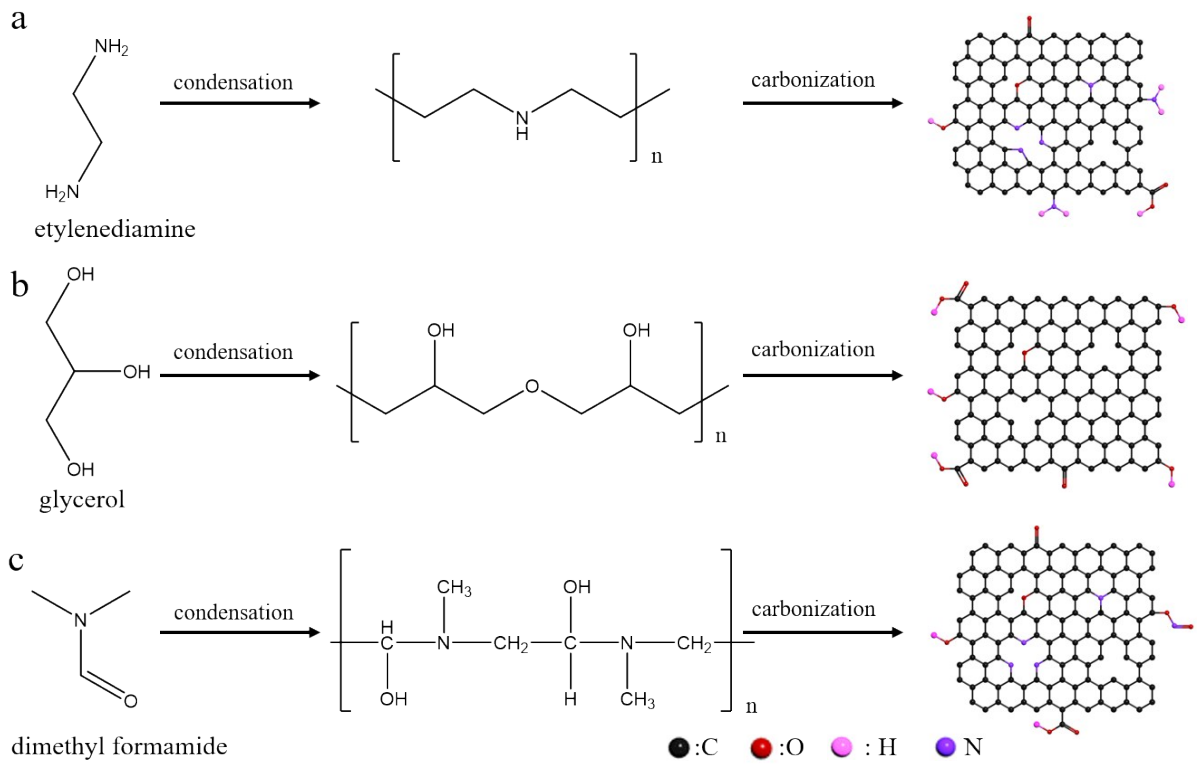

Fig. S4. Schematic illustration of grown mechanism of GQDs-En (a), GQDs-Gl (b) and GQDs-Dmf (c), respectively.

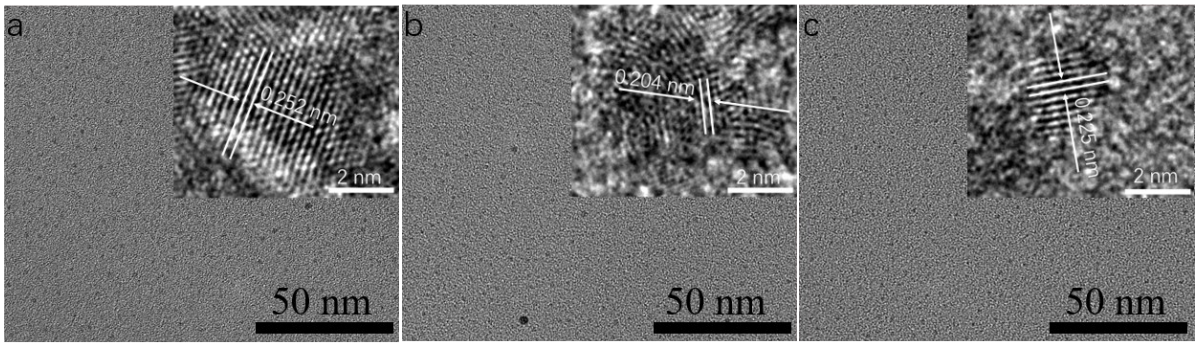

Fig. S5. (a-c) TEM and High-resolution TEM images (inset) of GQDs-En, GQDs-Gl, and GQDs-Dmf, respectively.

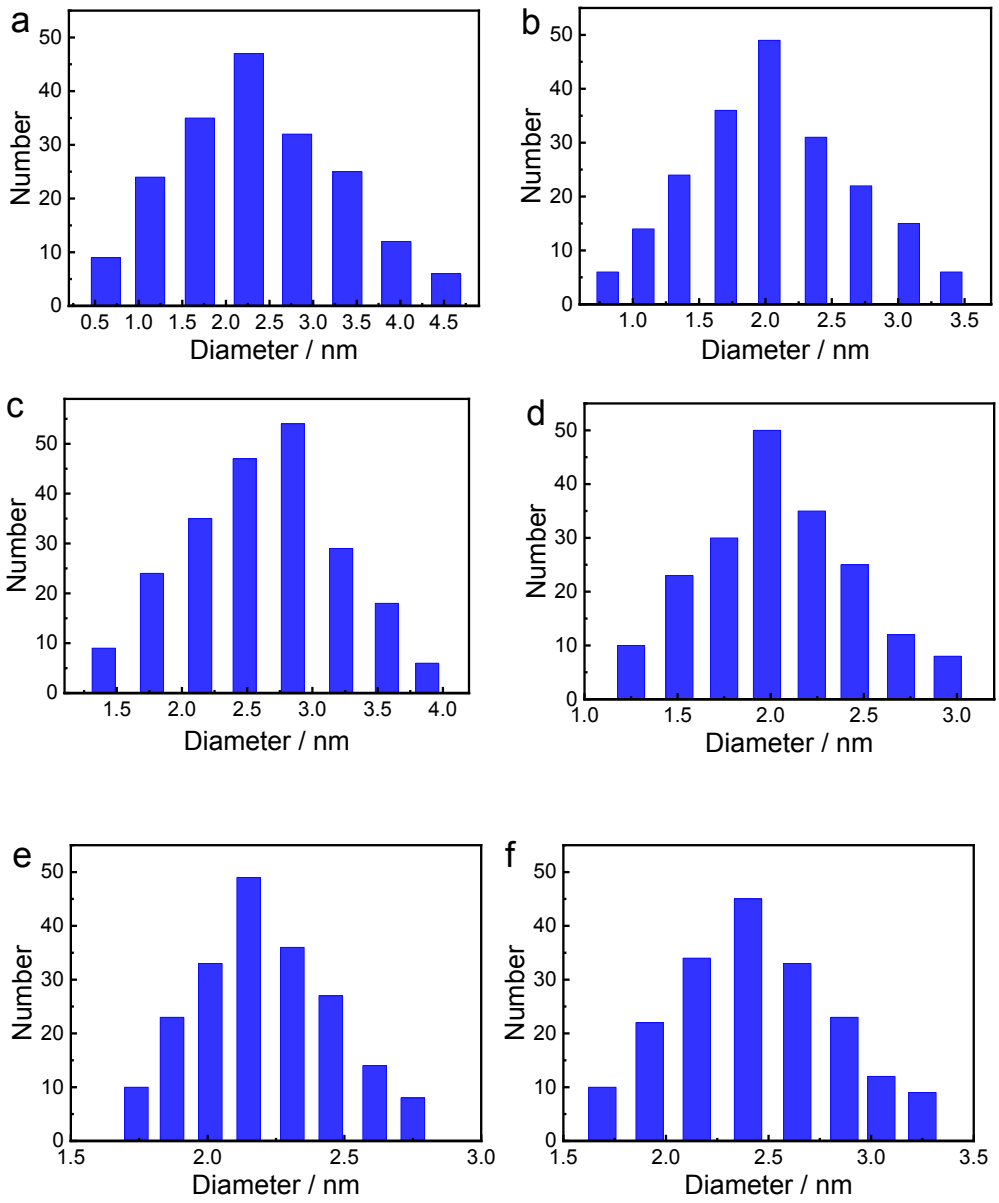

Fig. S6. Size distributions of (a) GQDs-Eg, (b) GQDs-Ac (c) GQDs-To (d) GQDs-En, (e) GQDs-Gl or GQDs-Dmf obtained by measuring ~200 GQDs, respectively.

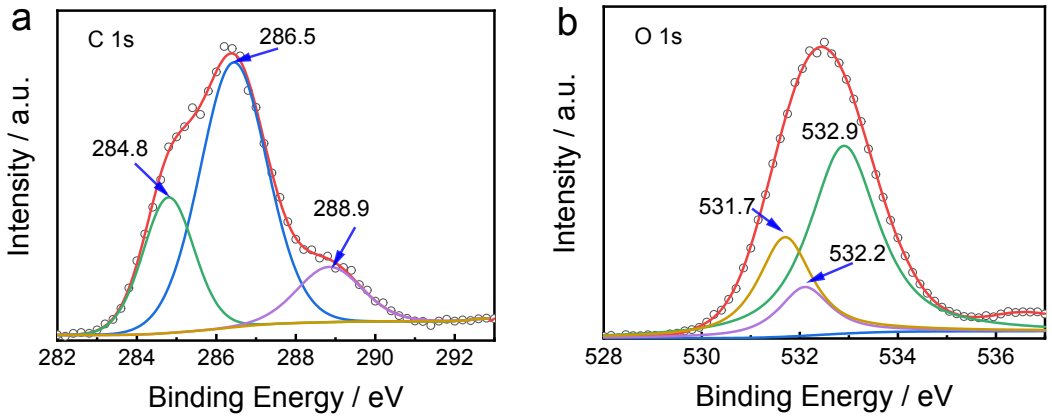

Fig. S7. Surface properties of GQDs-Eg. XPS high-resolution survey scan of C 1s (a) and O 1s (b). The C 1s peaks at 284.8, 286.5 and 288.9 eV are assigned to the presence of graphitic carbon, C-O (epoxy/ether) and carbonyl.[2] The O 1s peaks at 531.7, 532.2 eV and 532.9 eV are associated with C=O, C-OH, and C-O-C, respectively.[3]

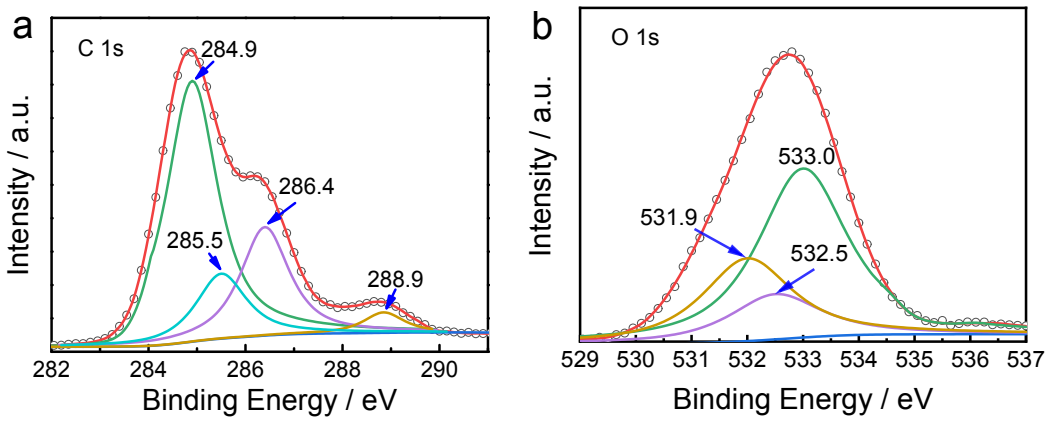

Fig. S8. Surface properties of GQDs-Ac. XPS high-resolution survey scan of C 1s (a) and O 1s (b). The C 1s peaks at 284.9, 285.5, 286.4, and 288.9 eV are assigned to C−C (sp^3)/C=C (sp^2), C−OH (sp^3), C-O (epoxy/ether, sp^3) and O−C=O (sp^2), respectively.[4] The O 1s peaks at 531.9, 532.5 and 533.0 eV are associated with C-O-C/C-OH, O-C-O and COOH, respectively.[3]

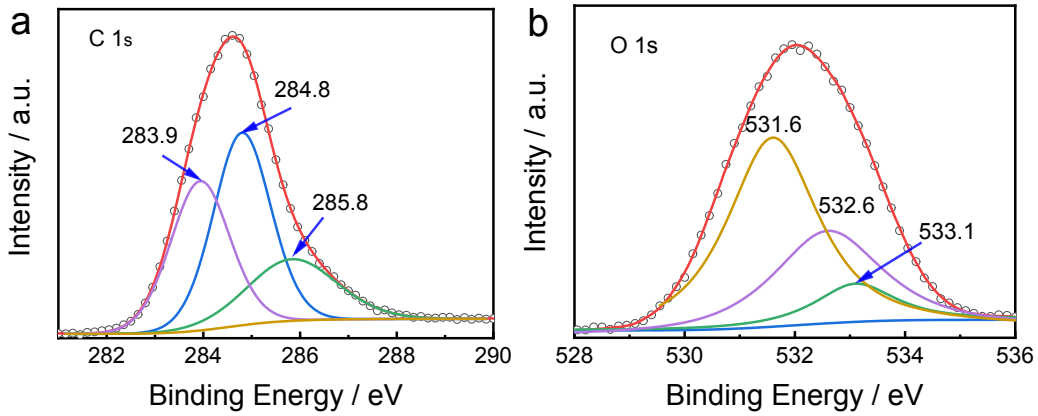

Fig. S9. Surface properties of GQDs-To. XPS high-resolution survey scan of C 1s (a) and O 1s (b). The C 1s peaks at 283.9, 284.8 and 285.8 eV are assigned to C=C, C-C and C−O, respectively.[5] The O 1s peaks at 531.6, 532.6 and 533.1 eV are associated with C=O, C-OH and C-O-C.[6].

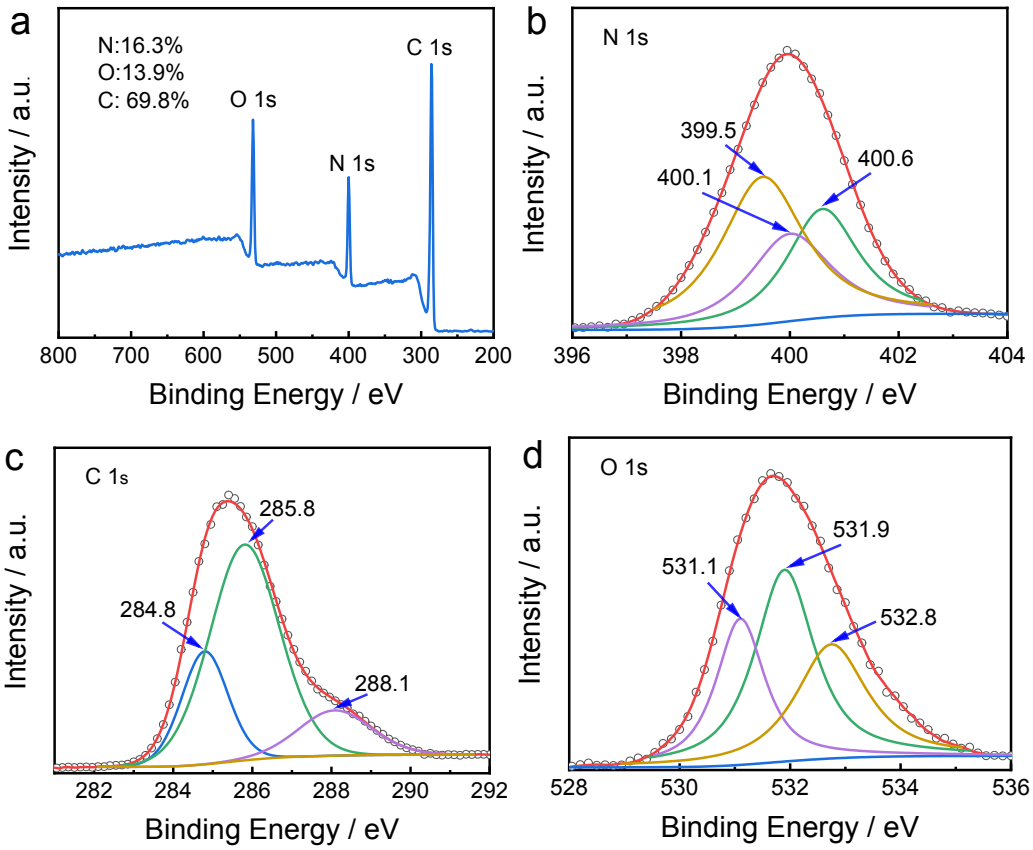

Fig. S10. Surface properties of GQDs-En. XPS scanning spectra (a) and XPS high-resolution survey scan of N 1s (b), C 1s (c) and O 1s (d). The N 1s spectra could be deconvoluted into three peaks assignable to pyridinic-N (399.5), graphitic N (400.1 eV), and pyrrolic N (400.6 eV).[7] The C 1s peaks at 284.8, 285.8 and 288.1 eV are assigned to C−C (sp^3)/C=C (sp^2), C−N (sp^3), and O−C=O (sp^2), respectively.[8] The O 1s peaks at 531.1, 531.9 and 532.8 eV are associated with C=O/O-H and C-O-C bonds.[9]

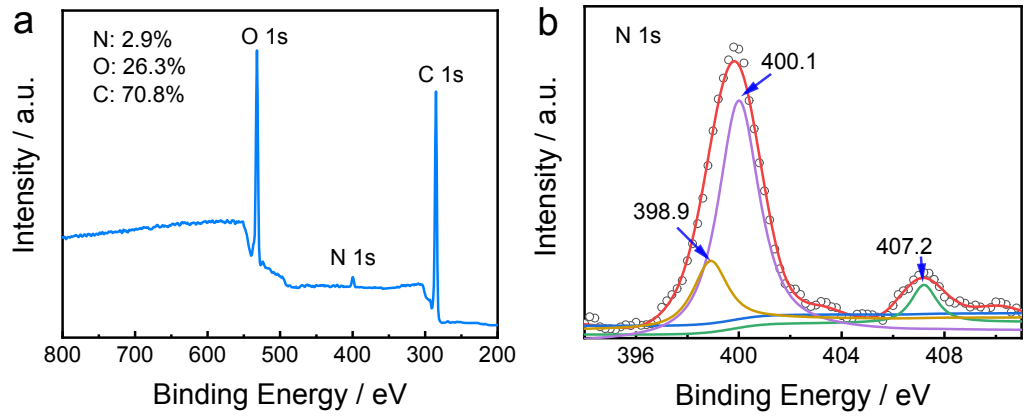

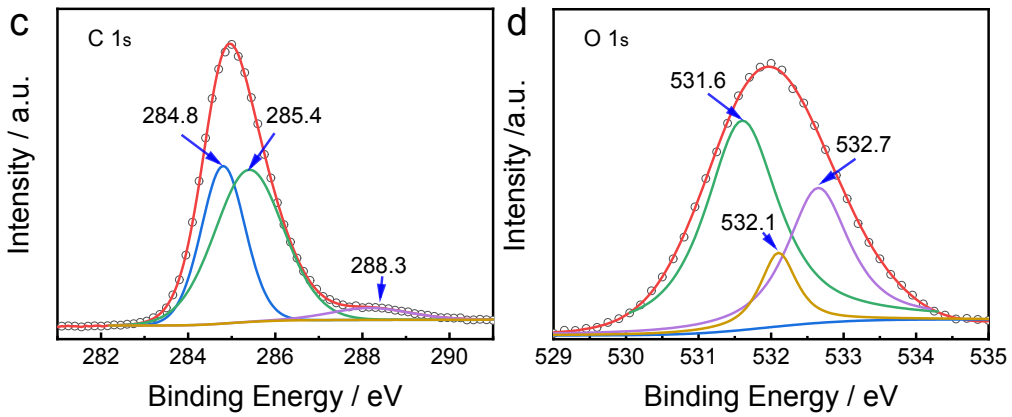

Fig. S11. Surface properties of GQDs-Dmf. XPS scanning spectra (a) and XPS high-resolution survey scan of N 1s (b), C 1s (c) and O 1s (d). The N 1s spectra could be deconvoluted into three peaks assignable to pyridinic-N (398.9), graphitic N (400.1 eV), and -NO_2 (407.2 eV).[10] The C 1s peaks at 284.8, 285.4, and 288.3 eV are assigned to graphitic carbon, C-N bond and C=O carbonyl carbon bond.[8] The O 1s peaks at 531.6, 532.1 and 532.7 eV are associated with C=O/O-H and C-O / C-NO_2 bonds.[9]

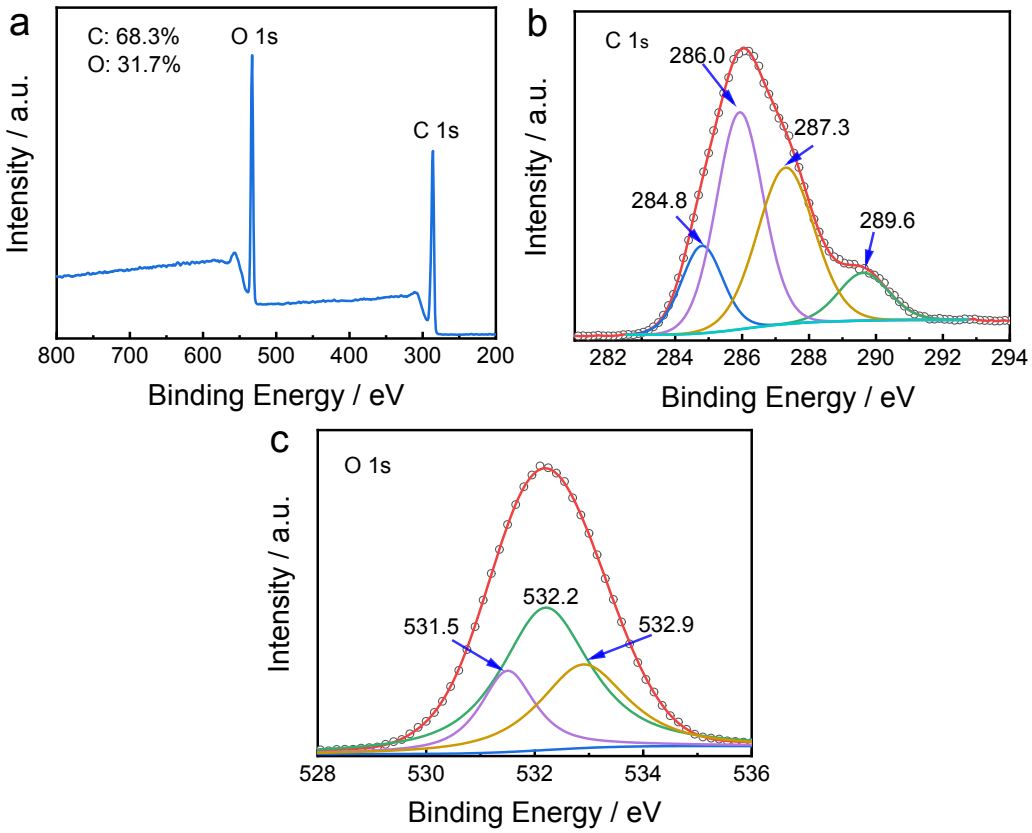

Fig. S12. Surface properties of GQDs-Gl. XPS scanning spectra (a) and XPS high-resolution survey scan of C 1s (b) and O 1s (c). The C 1s peaks at 284.8, 286.0, 287.3 and 289.6 eV are assigned to C=C/C-C, C-OH, C-O-C, and O-C=O.[11] The O 1s peaks at 531.5, 532.2 and 532.9 eV are associated with C=O, O-H, C-O-C bonds.[9]

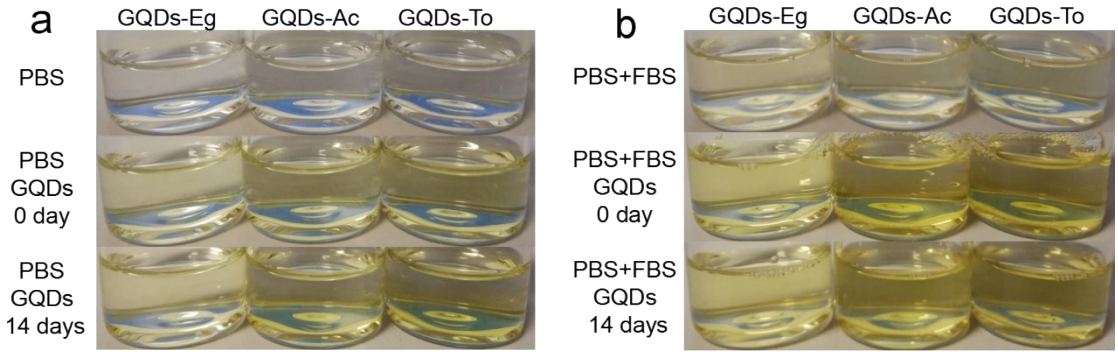

Fig. S13. The stability of GQDs dispersed in (a) PBS and (b) PBS containing 10% fetal bovine serum (FBS) under different time points.

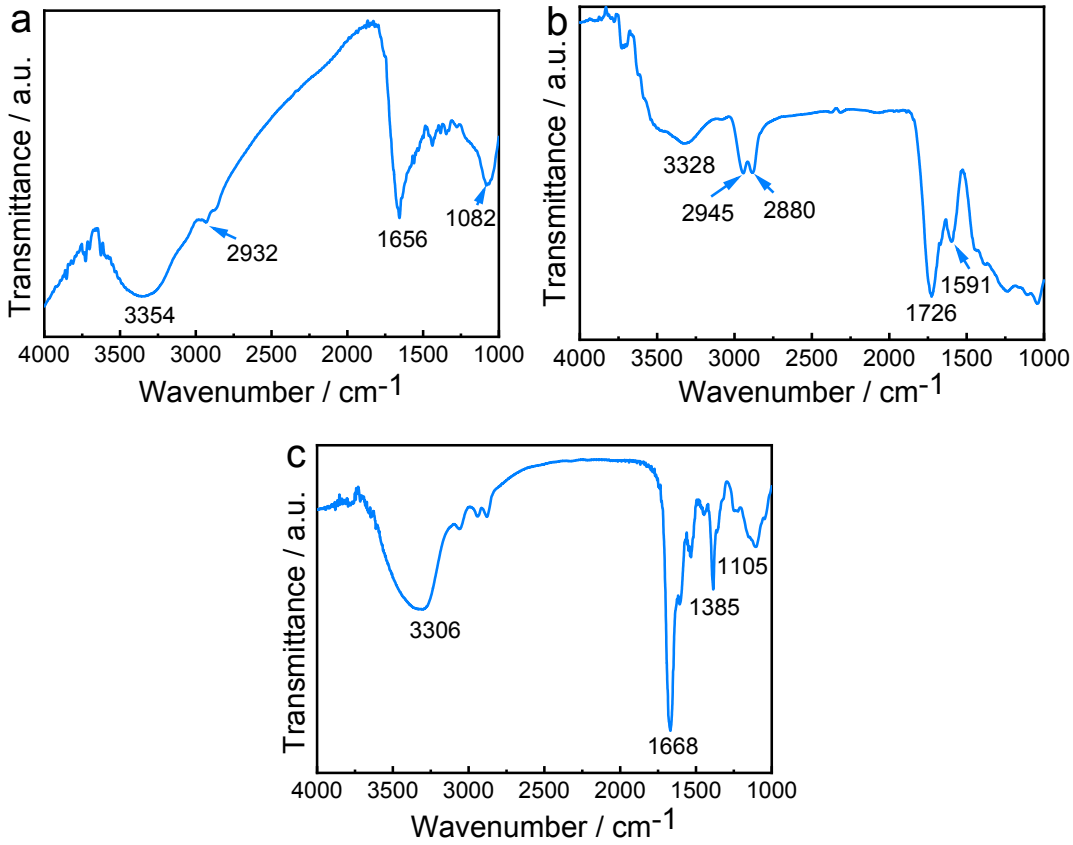

Fig. S14. FT-IR spectra of the as-synthesized GQDs-En (a), GQDs-Gl (b) and GQDs-Dmf (c), respectively.

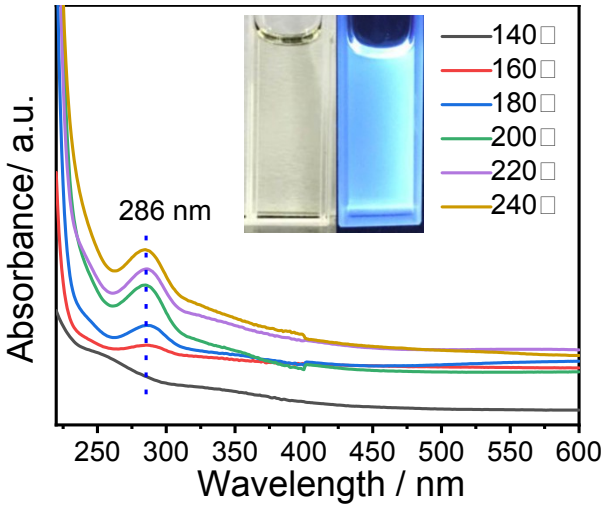

Fig. S15. UV-visible absorption spectra of GQDs-En synthesized at different temperature from 140 °C to 240 °C. The insets are optical pictures of GQDs-En synthesized at 220 °C under visible light (left) and UV light (right, 365 nm).

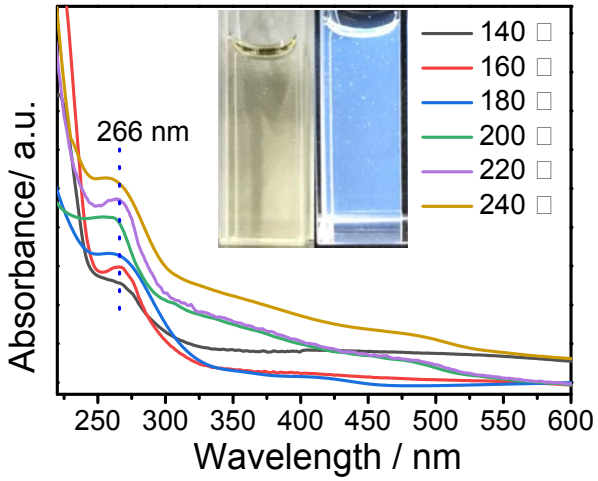

Fig. S16. UV-visible absorption spectra of GQDs-Gl synthesized at different temperature from 140 °C to 240 °C. The insets are optical pictures of GQDs-Gl synthesized at 220 °C under visible light (left) and UV light (right, 365 nm).

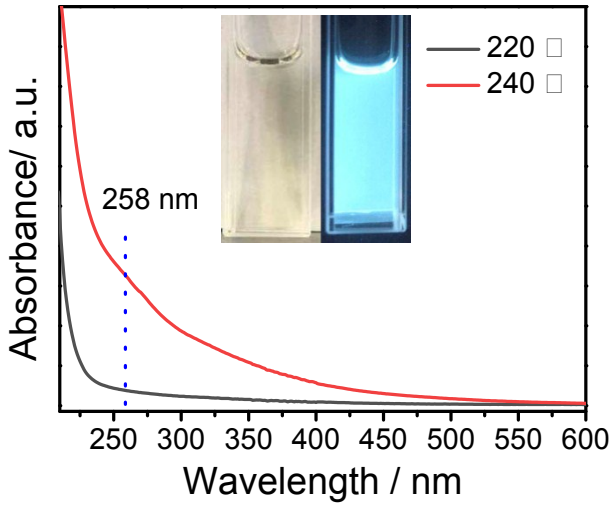

Fig. S17. UV-visible absorption spectra of GQDs-Dmf synthesized at different temperature from 220 °C to 240 °C. The insets are optical pictures of GQDs-Dmf synthesized at 220 °C under visible light (left) and UV light (right, 365 nm).

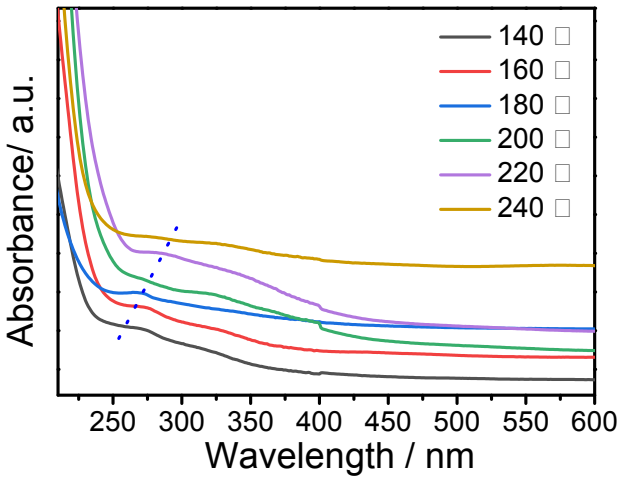

Fig. S18. UV-visible absorption spectra of GQDs-Eg synthesized at different temperature from 140 °C to 240 °C.

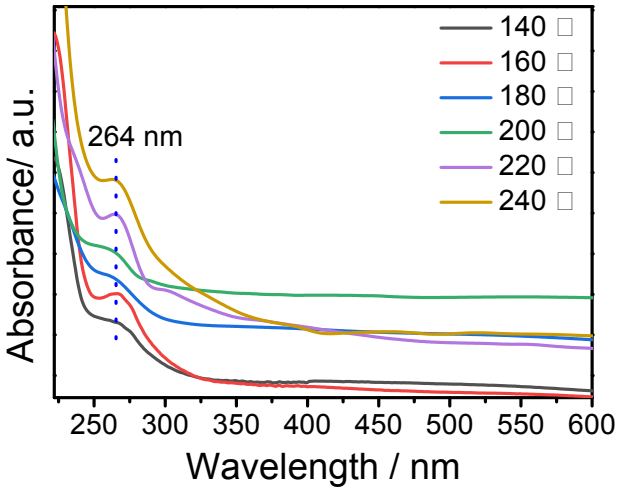

Fig. S19. UV-visible absorption spectra of GQDs-To synthesized at different temperature from 140 °C to 240 °C.

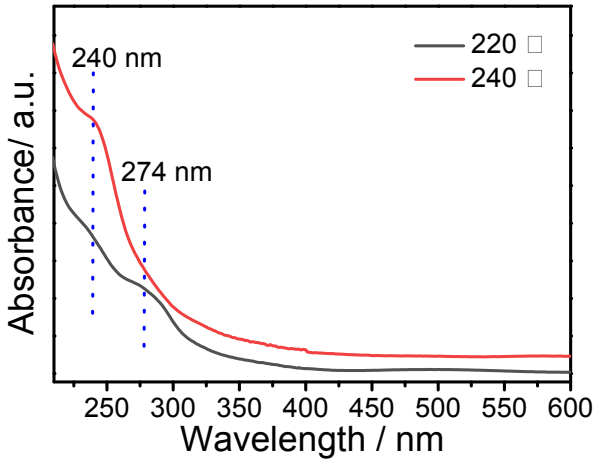

Fig. S20. UV-visible absorption spectra of GQDs-Ac synthesized at different temperature from 220 °C to 240 °C.

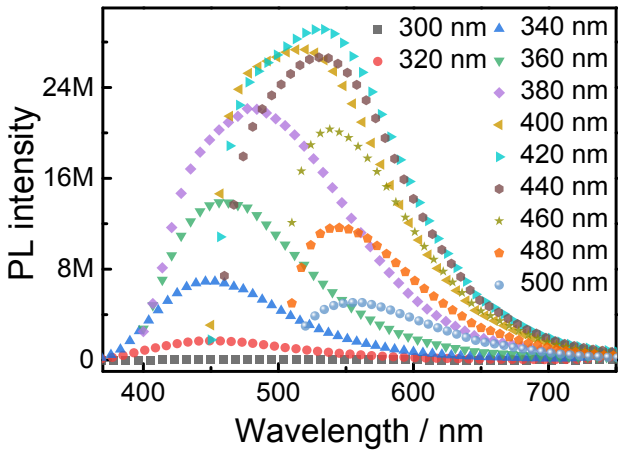

Fig. S21. PL spectra of GQDs-En synthesized at a temperature of 220 °C under different excitation wavelengths.

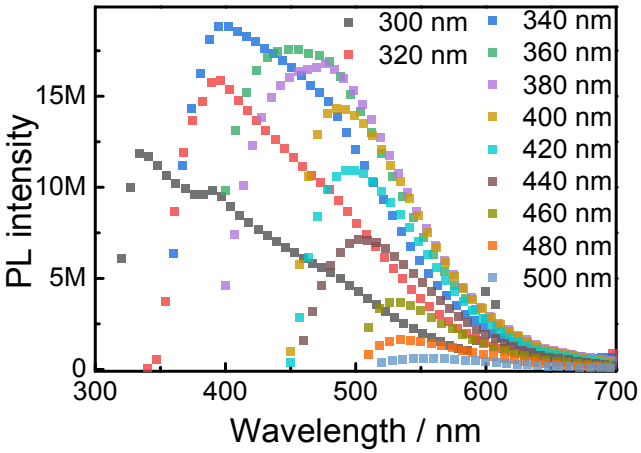

Fig. S22. PL spectra of GQDs-Gl synthesized at a temperature of 220 °C under different excitation wavelengths.

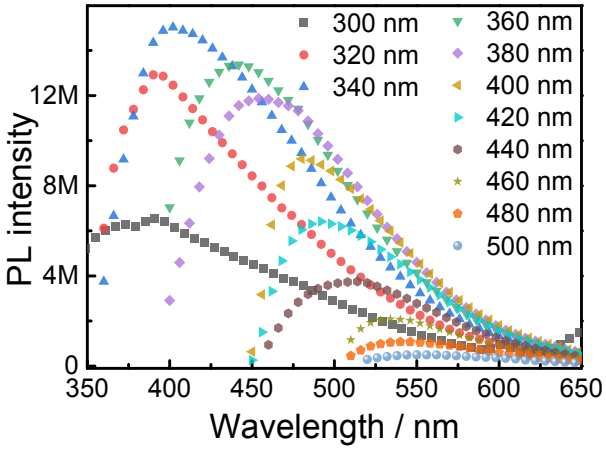

Fig. S23. PL spectra of GQDs-Dmf synthesized at a temperature of 220 °C under different excitation wavelengths.

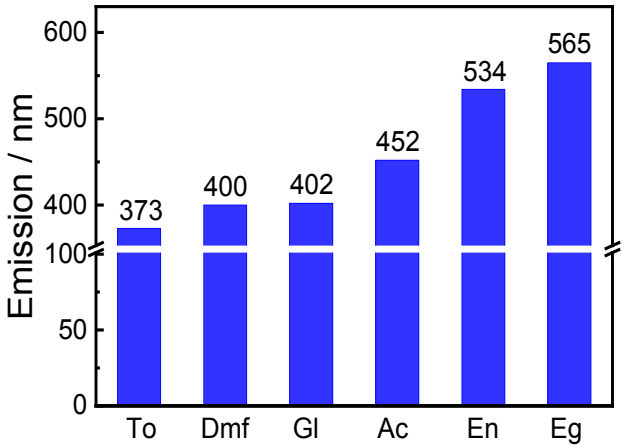

Fig. S24. Maximum PL emission position of the GQDs synthesized from different organic solvents at 220 °C.

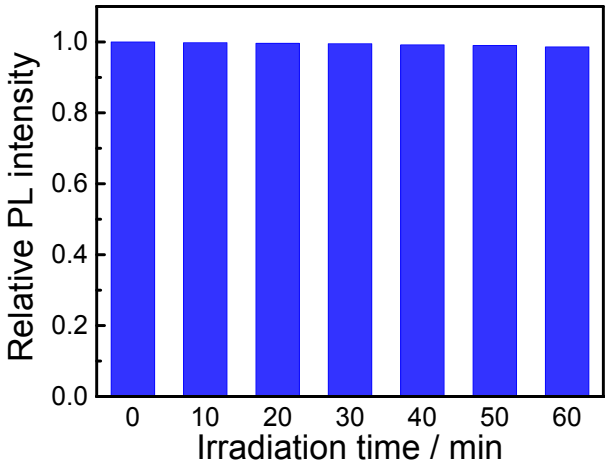

Fig. S25. Relative PL intensity change of emission peak (565 nm) of GQDs-Eg synthesized at a temperature of 220 °C at a excitation wavelength of 440 nm with different irradiation time.

Fig. S26. Representative laser scanning confocal microscopy images of Hela cells treated with PBS for 4 h under different excitation wavelengths. (a) 405 nm; (b) 488 nm; (c) 546 nm.

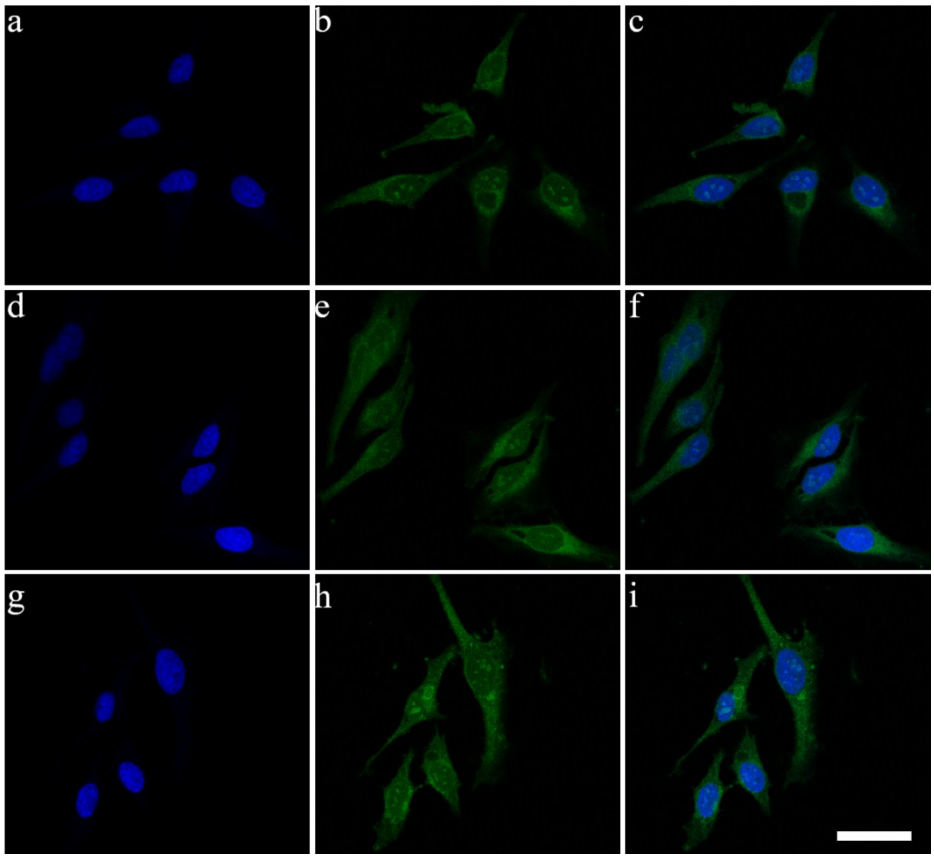

Fig. S27. Representative two-photon fluorescence cellular imaging. (a, d and g) DAPI nuclear stain, (b, e and h) two photon fluorescence, and (c, f and i) overlaid images of Hela cells incubated with GQDs-Eg, GQDs-Ac and GQDs-To. Excitation laser wavelength is 800 nm. The scale bar is 50 μm.

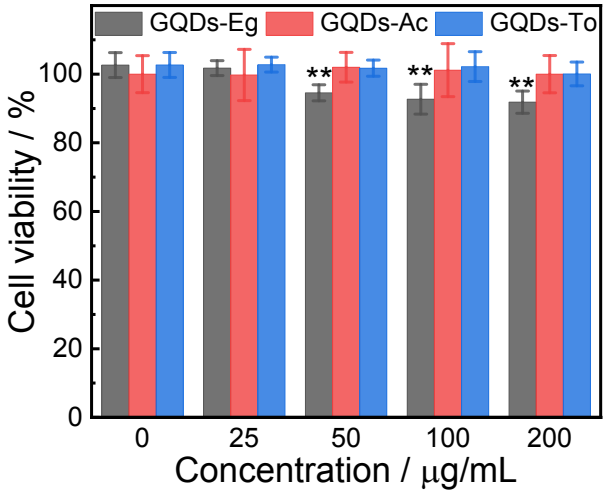

Fig. S28. In vitro cytotoxicity in NCI-H196 cells treated with GQDs-Eg, GQDs-Ac, and GQDs-To for 72 h.

References

1. Kuo, W. S.; Chen, H. H.; Chen, S. Y.; Chang, C. Y.; Chen, P. C.; Hou, Y. I.; Shao, Y. T.; Kao, H. F.; Lilian Hsu, C. L.; Chen, Y. C.; Chen, S. J.; Wu, S. R.; Wang, J. Y., Graphene quantum dots with nitrogen-doped content dependence for highly efficient dual-modality photodynamic antimicrobial therapy and bioimaging. *Biomaterials* **2017,** *120*, 185-194.
2. Lai, L.; Chen, L.; Zhan, D.; Sun, L.; Liu, J.; Lim, S. H.; Poh, C. K.; Shen, Z.; Lin, J., One-step synthesis of NH2-graphene from in situ graphene-oxide reduction and its improved electrochemical properties. *Carbon* **2011,** *49* (10), 3250-3257.
3. Zhou, H. Y.; Sui, Z. Y.; Liu, S.; Wang, H. Y.; Han, B. H., Nanostructured porous carbons derived from nitrogen-doped graphene nanoribbon aerogels for lithium-sulfur batteries. *J Colloid. Interface Sci.* **2019,** *541*, 204-212.
4. Quintana, M.; Spyrou, K.; Grzelczak, M.; Browne, W. R.; Rudolf, P.; Prato, M., Functionalization of graphene via 1,3-dipolar cycloaddition. *ACS Nano* **2010,** *4* (6), 3527-3533.
5. Xu, M.; He, G.; Li, Z.; He, F.; Gao, F.; Su, Y.; Zhang, L.; Yang, Z.; Zhang, Y., A green heterogeneous synthesis of N-doped carbon dots and their photoluminescence applications in solid and aqueous states. *Nanoscale* **2014,** *6* (17), 10307-10315.
6. Wang, H.; Zhuang, J.; Velado, D.; Wei, Z.; Matsui, H.; Zhou, S., Near-Infrared- and Visible-Light-Enhanced Metal-Free Catalytic Degradation of Organic Pollutants over Carbon-Dot-Based Carbocatalysts Synthesized from Biomass. *ACS Appl. Mater. Interfaces* **2015,** *7* (50), 27703-27712.
7. Fu, M.; Ehrat, F.; Wang, Y.; Milowska, K. Z.; Reckmeier, C.; Rogach, A. L.; Stolarczyk, J. K.; Urban, A. S.; Feldmann, J., Carbon Dots: A Unique Fluorescent Cocktail of Polycyclic Aromatic Hydrocarbons. *Nano Lett.* **2015,** *15* (9), 6030-6035.
8. Zhang, Q.; Deng, S.; Liu, J.; Zhong, X.; He, J.; Chen, X.; Feng, B.; Chen, Y.; Ostrikov, K., Cancer‐Targeting Graphene Quantum Dots: Fluorescence Quantum Yields, Stability, and Cell Selectivity. *Adv. Funct. Mater.* **2018**, 1805860.
9. Dong, Y.; Pang, H.; Yang, H. B.; Guo, C.; Shao, J.; Chi, Y.; Li, C. M.; Yu, T., Carbon-based dots co-doped with nitrogen and sulfur for high quantum yield and excitation-independent emission. *Angew Chem. Int. Ed. Engl.* **2013,** *52* (30), 7800-7804.
10. Lee, S. H.; Kim, D. Y.; Lee, J.; Lee, S. B.; Han, H.; Kim, Y. Y.; Mun, S. C.; Im, S. H.; Kim, T. H.; Park, O. O., Synthesis of Single-Crystalline Hexagonal Graphene Quantum Dots from Solution Chemistry. *Nano Lett.* **2019,** *19* (8), 5437-5442.
11. Wu, M.; Zhan, J.; Geng, B.; He, P.; Wu, K.; Wang, L.; Xu, G.; Li, Z.; Yin, L.; Pan, D., Scalable synthesis of organic-soluble carbon quantum dots: superior optical properties in solvents, solids, and LEDs. *Nanoscale* **2017,** *9* (35), 13195-13202.
12. Mattevi, C.; Eda, G.; Agnoli, S.; Miller, S.; Mkhoyan, K. A.; Celik, O.; Mastrogiovanni, D.; Granozzi, G.; Garfunkel, E.; Chhowalla, M., Evolution of Electrical, Chemical, and Structural Properties of Transparent and Conducting Chemically Derived Graphene Thin Films. *Adv. Funct. Mater.* **2009,** *19* (16), 2577-2583.
13. Fei, X.; Neilson, J.; Li, Y.; Lopez, V.; Garrett, S. J.; Gan, L.; Gao, H. J.; Gao, L., Controlled Synthesis of Nitrogen-Doped Graphene on Ruthenium from Azafullerene. *Nano Lett.* **2017,** *17* (5), 2887-2894.
14. Kang, S. J.; Mori, T.; Narizuka, S.; Wilcke, W.; Kim, H. C., Deactivation of carbon electrode for elimination of carbon dioxide evolution from rechargeable lithium-oxygen cells. *Nat. Commun.* **2014,** *5*, 3937.
15. Tang, L.; Ji, R.; Cao, X.; Lin, J.; Jiang, H.; Li, X.; Teng, K. S.; Luk, C. M.; Zeng, S.; Hao, J.; Lau, S. P., Deep ultraviolet photoluminescence of water-soluble self-passivated graphene quantum dots. *ACS Nano* **2012,** *6* (6), 5102-5110.
16. Shin, H. J.; Kim, K. K.; Benayad, A.; Yoon, S. M.; Park, H. K.; Jung, I. S.; Jin, M. H.; Jeong, H. K.; Kim, J. M.; Choi, J. Y.; Lee, Y. H., Efficient Reduction of Graphite Oxide by Sodium Borohydride and Its Effect on Electrical Conductance. *Adv. Funct. Mater.* **2009,** *19* (12), 1987-1992.